Energy-Autonomous Supply-Sensing Biosensor Platform Using CMOS Electronics and Biofuel Cells

Kiichi Niitsu

1 Introduction

Ensuring stable energy is one of the most important challenges in the current wearable and implantable healthcare devices associated with big-data-based analysis (Fig. 1). To address this issue, many attempts such as developments of battery, wireless power delivery, and energy harvesting have been reported. Although the technical improvement has been rapid, none of these methods fully satisfy the requirement. Battery is unsuitable for use near a human body due to its inherent danger. Wireless power delivery requires large-size power-receiving antenna. Energy harvesting is unstable for healthcare application. Additionally, the latter two approaches require area-consuming power management unit such as power receiver and AC-DC converter that increase cost.

To satisfy the requirement, biofuel cells are intensely developed such as for transdermal iontophoresis patch [1] and brain-machine interface [2]. Biofuel cells are safe, stable, and do not require an antenna or an AC-DC converter. Additionally, the value of the obtained energy from a human body can be used as biosensing data, and, thus, sensor electrodes and front ends become unnecessary. Among the biofuel cell types, the organic biofuel cell [1] is especially promising because it is cheap and environment friendly, which enables disposable healthcare. However, the output supply voltage of a biofuel cell is usually lower than 0.4 V, and conventional circuits cannot operate using a biofuel cell without power management circuits such as up-converter. Thus, new circuit technique must be developed for converterless operation.

K. Niitsu (✉)
Department of Electrical Engineering and Computer Science, Nagoya University, C3-1(631), Furo-Cho, Chikusa-Ku, Nagoya, 464-8603, Japan
e-mail: niitsu@nuee.nagoya-u.ac.jp

H. Yasuura et al. (eds.), *Smart Sensors at the IoT Frontier*,
DOI 10.1007/978-3-319-55345-0_2

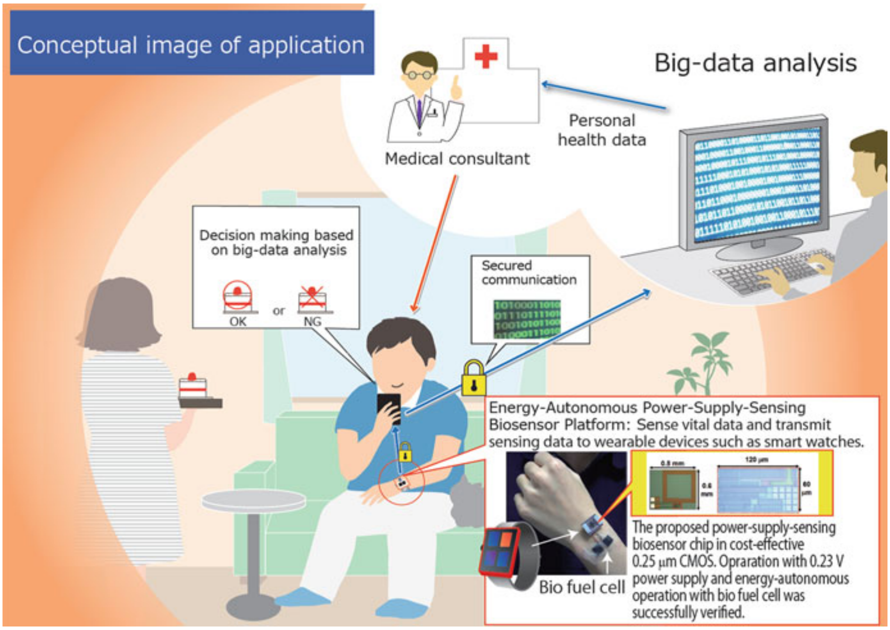

Fig. 1 Conceptual image of the application of the proposed work. The target application is big-data-based healthcare. The proposed energy-autonomous biosensor transmits vital data to the wearable device

The current chapter introduces a supply-sensing biosensor platform using a biofuel cell and a 0.23-V 0.25-μm zero-V_{th} all-digital CMOS supply-controlled ring oscillator (SCRO) with a current-driven pulse-interval-modulated inductive-coupling transmitter (Fig. 2). Compared with conventional architecture [3, 4], the occupied area and required power can be dramatically reduced. To realize transmit sensing data to the wearable device without power-hungry security protection circuits, a proximity inductive-coupling transmitter is employed.

To verify the effectiveness of the proposed approach, a test chip was fabricated using the cost-competitive legacy 0.25-μm CMOS technology. The measured results show successful operation with a 0.23-V power supply, which is the lowest supply voltage ever reported. In addition to the chip functional test, energy-autonomous operation using a biofuel cell was successfully demonstrated.

This chapter is organized as follows: the proposed energy-harvesting and biosensor platform is introduced in Sect. 2. The design of the prototype CMOS sensor and the measurement setup are summarized in Sect. 3. Sections 4 and 5 present the measurement results and demonstration of the energy-autonomous operation. Section 6 concludes this chapter.

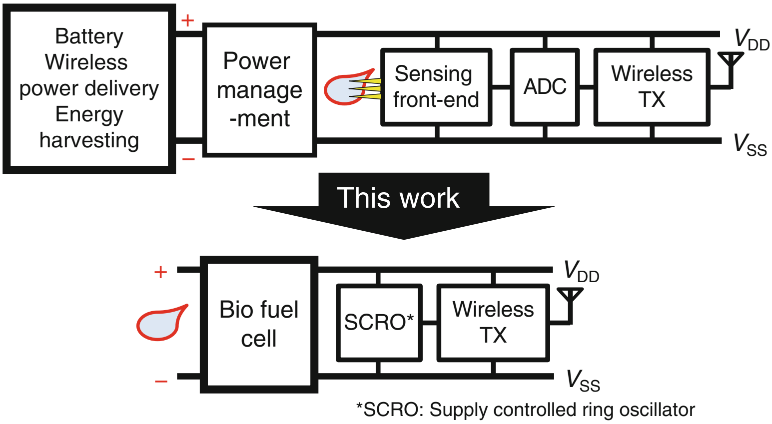

Fig. 2 Performance comparison with the state-of-the-art proximity communications

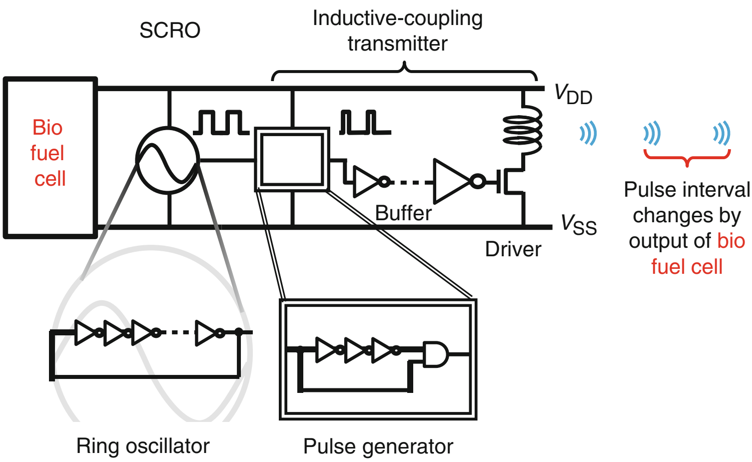

Fig. 3 Circuit diagram of the proposed supply-sensing biosensor

2 Supply-Sensing Biosensor Platform

2.1 Principle of Supply-Sensing Biosensor Platform

Figure 3 shows the circuit diagram of the proposed supply-sensing biosensor platform. The proposed sensor platform consists of three parts: biofuel cells, SCRO, and an inductive-coupling transmitter. By eliminating the area-hungry power management circuits, sensing front-end circuit, and power-hungry analog-to-digital converters (ADC), the occupied area and required power can be dramatically reduced.

To minimize the supply voltage, an all-digital and current-driven architecture was employed. By implementing the proposed architecture using zero-V_{th} transistors, a low-supply voltage of less than 0.4 V was made feasible. Because the supply-sensing scheme is unsuitable for pulse amplitude modulation owing to its nature, time-domain modulation must be employed. To minimize power consumption, pulse-interval modulation (PIM) was employed in this work.

2.2 Biofuel Cell

In the proposed platform, the biofuel cell is the key component that provides two functions: one is energy harvesting, and the other is front-end sensing. Typical biofuel cells can generate voltage of less than 0.4 V [1, 2]. Thus, to realize energy-autonomous operation without area-consuming power management circuits such as up-converters, the circuits must operate with a supply voltage of less than 0.4 V.

In order for biofuel cells to function as both a power source and sensing front end, the anode and cathode must be designed carefully as follows. Unlike typical biosensors based on one transducer, the proposed supply-sensing biosensor uses two transducers (anode and cathode). Thus, if the output power depends on unintended transducers, the proposed device cannot function as a sensor even if it functions well as power source.

In the case of our prototype fructose supply-sensing sensor, we use the following reactions. In the anode, the output current depends on fructose concentration. In the cathode, the output current depends on oxygen concentration. To sense fructose, the total output current must depend on not oxygen but fructose, which we achieve by adjusting the sizes of the anode and cathode.

2.3 Supply-Controlled Ring Oscillator (SCRO)

To realize PIM, the supply voltage must be modulated to pulse interval. To enable low-voltage operation, we implemented an SCRO. The SCRO consists of normal ring oscillator with PMOS and NMOS. The number of stages was determined by considering the trade-off between area overhead and power consumption. In this work, to minimize the occupied area, the number of stages of inverter gates was designed to be as small as possible while maintaining effective operation.

2.4 Inductive-Coupling Transmitter

For the wireless transmitter, we implemented a current-driven inductive-coupling transmitter. By considering the limited power budget, proximity communication without any security protection was adopted. Proximity communication can be

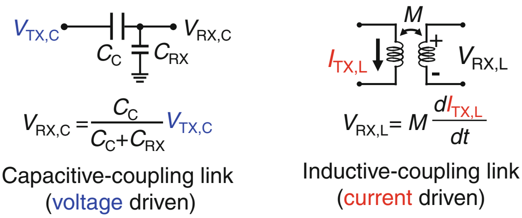

Fig. 4 Operating principle of the proximity communication

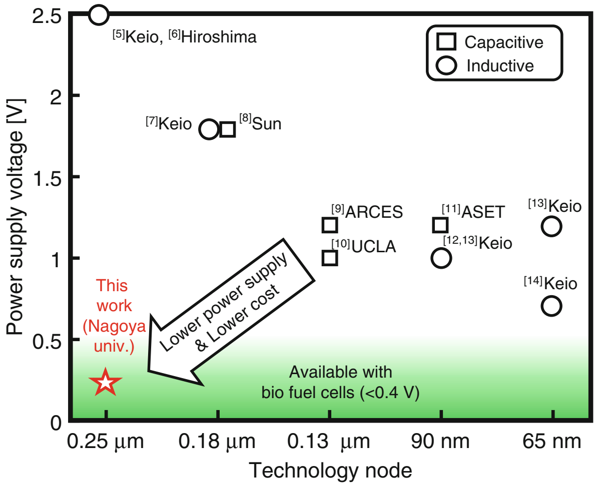

Fig. 5 Performance comparison with the state-of-the-art proximity communications

categorized into two approaches: one is the capacitive-coupling link, and another is the inductive-coupling link. Figure 4 shows their conceptual operating principle. The obtained voltage at the receiver side of capacitive link is determined by the ratio of the coupled capacitance to the total capacitance. Thus, a received voltage that is higher than the transmit voltage cannot be obtained.

In contrast, the received voltage in the inductive-coupling link is determined by a multiple of the slew rate of the transmit current and the mutual inductance. A high received voltage can be obtained even with a low supply-voltage transmitter. Biofuel cells can generate larger current at lower voltage owing to its characteristic; thus, the current-driven inductive-coupling link is preferred.

To minimize power supply voltage while enjoying the advantage of the inductive-coupling link, the proposed inductive-coupling transmitter was designed to be as simple as possible, as shown in Fig. 3, which consisted of a pulse generator, buffers, driver, and inductor. The pulse generator consisted of an inverter chain and an AND gate, which converts the clock signal to a low-duty pulse signal.

Figure 5 shows the performance comparison of the proposed method with the state-of-the-art proximity communications. The literature shows a trade-off between power supply voltage and technology node. The lowest supply voltage was 0.7 V [14] for the clock-based synchronous inductive-coupling link, and none of the conventional proximity communications could satisfy the requirement. This work achieved the lowest supply using the most cost-competitive technology node.

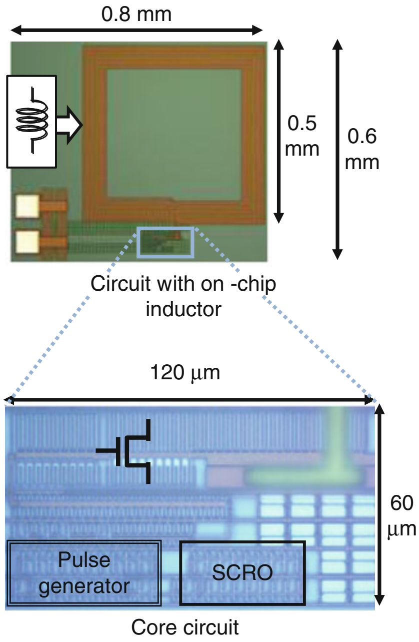

Fig. 6 Chip microphotograph of the proposed supply-sensing biosensor platform in 0.25-µm CMOS

3 Test Chip Design and Measurement Setup

To verify the effectiveness of the proposed approach, a test chip was fabricated using a cost-competitive 0.25-µm CMOS technology. Figure 6 shows the microphotograph of the test chip. The occupied footprints of the core circuit without an on-chip inductor and the entire circuit with an on-chip inductor were 60×120 µm and 0.6×0.8 mm, respectively. The test chip was assembled in a ceramic package. The diameter of the inductor is 0.5 mm.

The measurement setup is shown in Fig. 7. Only two electrical signals, namely, V_{DD} and V_{SS}, were supplied from the power supply (Keysight Technologies, E3632A). To verify the transmitter operation using magnetic detection, a magnetic field probe (Langer, H-Field probe MFA-K 0.1-12, 0.1–6 GHz) and a bias tee (Langer, Bias Tee) were employed. The waveform was obtained using a sampling oscilloscope (Keysight Technologies, DSO6102A).

4 Measurement Results

Figure 8 shows the measured current-consumption dependence on the supply voltage. The operation under a 0.23-V power supply was successfully verified. The 0.23-V supply is sufficiently low for energy-autonomous operation using a

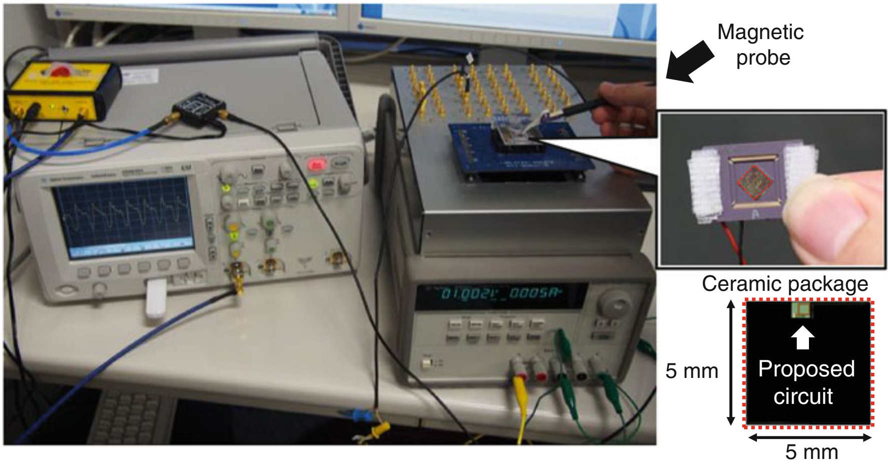

Fig. 7 Measurement setup

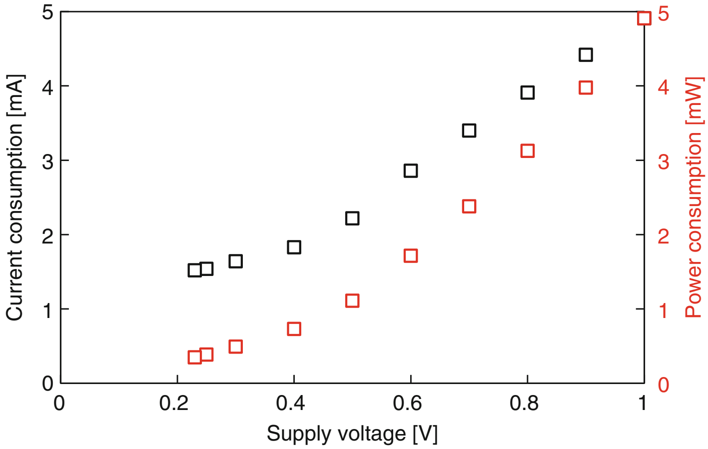

Fig. 8 Measured current-consumption dependence on the supply voltage. A 0.23-V operation was verified

biofuel cell. This is the lowest supply voltage ever reported among proximity communications. Because the drain current of a zero-V_{th} transistor is proportional to the square of the gate-source voltage, V_{GS}, from 0 to 0.4 V and is proportional to V_{GS} from 0.4 V, the current-consumption trend changes at 0.4 V.

The measured current consumption at 0.23-V power supply is 1.52 mA. The measured power is 0.35 mW. This power can be obtained by a 1 cm^2 of biofuel cell [1]. Owing to the conservative design, the current consumption in this technology node was not minimized. By optimizing the design parameters, further power reduction can be realized.

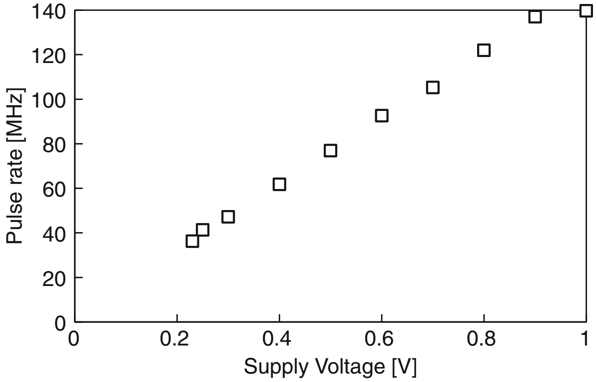

Fig. 9 Measured pulse rate dependence on the supply voltage

Figure 9 shows the frequency of the output pulse from the magnetic field dependence on the supply voltage. The pulse rate decreased with the decrease in the supply voltage. An almost linear relationship between the pulse rate and supply voltage was verified. This linear characteristic will contribute to develop wide-range sensor. Besides, it will also enable easy and accurate calibration.

5 Energy-Autonomous Operation

5.1 Performance of Organic Biofuel Cell

To verify the effectiveness of the proposed platform, energy-autonomous operation using organic biofuel cell [1] was demonstrated. The biofuel cell has a cloth-like feature. The enzymes for energy generation were immobilized to the biofuel cell. Figure 10 shows a summary of the measured performance of the biofuel cell.

The biofuel cell generates energy from fructose. The size of the biofuel cell is 1-cm square. The peak power can be obtained at 0.3–0.4 V, which is a typical characteristic of biofuel cells [1, 2]. The measurement was performed using a three-electrode system (BSA, 730C electrochemical analyzer).

5.2 Demonstration of Energy-Autonomous Biosensing

Figure 11 shows a successful energy-autonomous operation using biofuel cell. By dipping the biofuel cell into a fructose solution, the circuit transmitted a magnetic field, and its waveform appeared on the oscilloscope. This work is the first demonstration of an energy-autonomous proximity transmission using biofuel cells.

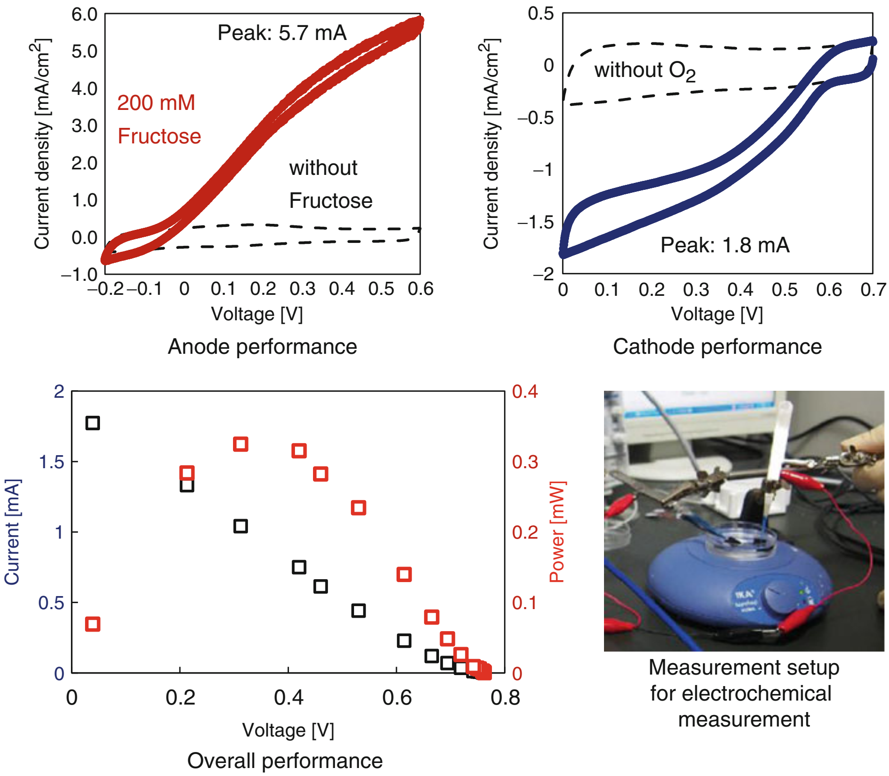

Fig. 10 Measured performance of the biofuel cell and its measurement setup

Figure 12 shows a summary of the energy-autonomous operation. Figure 12a shows the output voltage and current of the biofuel cell as a function of fructose concentration. The voltage and current increased as the fructose concentration increased. Figure 12b shows the measured pulse rate of the output magnetic field from the proposed biosensor platform. The pulse rate increased as the fructose concentration increased. These results agree well with the performance of the platform shown in Fig. 9. From these measured results, we have successfully confirmed the feasibility of the proposed energy-autonomous supply-sensing biosensor platform.

6 Discussion

This chapter demonstrates that the proposed supply-sensing sensor platform can be applied to fructose sensing. But, the proposed sensor platform can be applied to wide applications. Today's CMOS bioelectronics enables various kinds of biosensing [15–25]. Thus, by combining the proposed sensor platform and the present

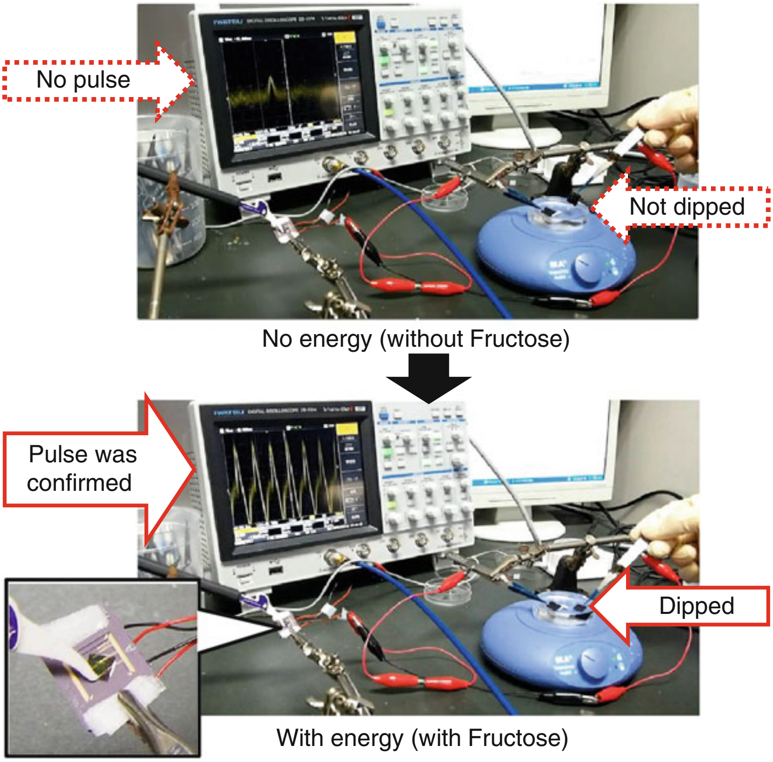

Fig. 11 Demonstration of energy-autonomous operation using organic biofuel cell. Only when dipping the biofuel cell into fructose solution, the proposed biosensor transmits magnetic pulse

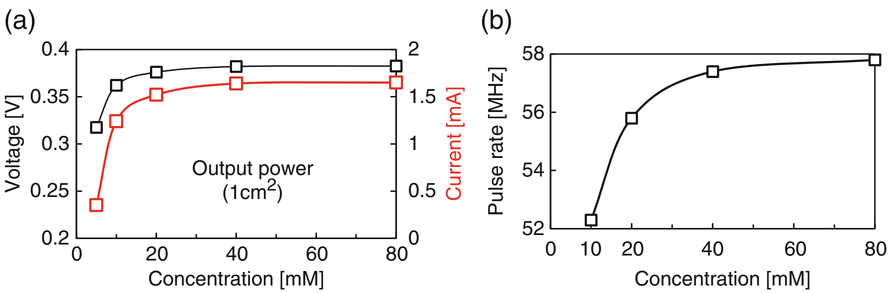

Fig. 12 Measured output voltage from biofuel cell (**a**) and measured pulse rate dependence on fructose concentration (**b**)

CMOS bioelectronics, energy-autonomous smart biosensor can be emerged. Furthermore, the proposed technique is familiar with CMOS scaling because it utilizes time-domain processing [26–30] and current-driven inductive-coupling inter-chip communication [31–37]. Future CMOS scaling will enhance the feasibility and effectiveness of the proposed sensor platform.

7 Conclusion

An energy-autonomous, disposable, supply-sensing biosensor platform has been demonstrated. The platform is based on a biofuel cell and a zero-V_{th} all-digital CMOS supply-controlled ring oscillator with a current-driven pulse-interval-modulated inductive-coupling transmitter that enables operation under low-power supply voltage using legacy CMOS technology. The measurement using a 0.25-μm CMOS prototype chip successfully demonstrated wireless transmission under a 0.23-V power supply, which is the lowest power supply proximity transmitter ever reported. Additionally, an energy-autonomous operation using an organic biofuel cell was successfully verified.

Acknowledgments This research was financially supported by JST, PRESTO, by a Grant-in-Aid for Scientific Research (S) (Nos. 20226009, 25220906, 26220801), Grants-in-Aid for Young Scientists (A) (No. 16H06088) from the Ministry of Education, Culture, Sports, Science and Technology of Japan, by the Strategic Information and Communications R&D Promotion Programme (Nos. 121806006, 152106004) of the Ministry of Internal Affairs and Communications, Japan, by TOYOTA RIKEN, and by The Nitto Foundation. The fabrication of CMOS chips was supported by Taiwan Semiconductor Manufacturing Co., Ltd. (TSMC, Taiwan), and the VLSI Design and Education Center (VDEC), University of Tokyo in collaboration with Synopsys, Inc. and Cadence Design Systems, Inc.

References

1. Ogawa, Y., Nishizawa, M., et al.: Organic transdermal iontophoresis patch with built-in biofuel cell. Adv. Healthc. Mater. **4**(4), 506–510 (2015)
2. Rapoport, B.I., et al.: A glucose fuel cell for implantable brain–machine interfaces. PLoS ONE. **7**(6), e38436 (2012)
3. Liao, Y.-T., et al.: A 3-μW CMOS glucose sensor for wireless contact-lens tear glucose monitoring. IEEE J. Solid-State Circ. **47**(1), 335–344 (2012)
4. Komori, H., Niitsu, K., Nakazato, K., et al.: An extended-gate CMOS sensor array with enzyme-immobilized microbeads for redox-potential glucose detection. In: IEEE Biomedical Circuits and Systems Conf, pp. 464–467 (2014)
5. Miura, N., et al.: A 195Gb/s 1.2W 3D-stacked inductive inter-chip wireless superconnect with transmit power control scheme. In: Proc. IEEE ISSCC, pp. 264–265 (2005)
6. Iwata, A., et al.: A 3D integration scheme utilizing wireless interconnections for implementing hyper brains. In: Proc. IEEE ISSCC, pp. 368–369 (2007)
7. Miura, N., et al.: A 1 Tb/s 3 W inductive-coupling transceiver for 3D-stacked inter-chip clock and data link. IEEE J. Solid State Circuits. **42**(1), 111–122 (2007)

8. Hopkins, D., et al.: Circuit techniques to enable 430Gb/s/mm^2 proximity communication. In: Proc. IEEE ISSCC, pp. 368–369 (2007)
9. Fazzi, A., et al.: 3D capacitive interconnections with mono- and bi-directional capabilities. In: Proc. IEEE ISSCC, pp. 356–357 (2007)
10. Gu, Q., et al.: Two 10Gb/s/pin low-power interconnect methods for 3D ICs. In: Proc. IEEE ISSCC, pp. 448–449 (2007)
11. Daito, M., et al.: Capacitively coupled non-contact probing circuits for membrane-based wafer-level simultaneous testing. In: Proc. IEEE ISSCC, pp. 144–145 (2010)
12. Niitsu, K., et al.: A 65fJ/b inter-chip inductive-coupling data transceivers using charge-recycling technique for low-power inter-chip communication in 3D system integration. IEEE Trans. Very Large Scale Integration (VLSI) Syst. pp. 1285–1294 (2012)
13. Niitsu, K., et al.: An inductive-coupling link for 3D integration of a 90nm CMOS processor and a 65nm CMOS SRAM. In: Proc. IEEE ISSCC, pp.480–481 (2009)
14. Miura, N., et al.: A 0.55 V 10 fJ/bit inductive-coupling data link and 0.7 V 135 fJ/cycle clock link with dual-coil transmission scheme. IEEE J. Solid State Circ., 965–973 (2011)
15. K. Niitsu, A. Kobayashi, Y. Ogawa, M. Nishizawa, K. Nakazato: An energy-autonomous, disposable, big-data-based supply-sensing biosensor using bio fuel cell and 0.23-V 0.25-μm zero-V_{th} all-digital CMOS supply-controlled ring oscillator with inductive transmitter. In: Proc. IEEE Biomed. Circ. Syst. Conf. pp. 595–598 (2015)
16. Niitsu, K., Ota, S., Gamo, K., Kondo, H., Hori, M., Nakazato, K.: Development of microelectrode arrays using electroless plating for CMOS-based direct counting of bacterial and HeLa cells. IEEE Trans. Biomed. Circ. Syst. **9**(5), 607–619 (2015)
17. Kuno, T., Niitsu, K., Nakazato, K.: Amperometric electrochemical sensor array for on-chip simultaneous imaging. Jpn. J. Appl. Phys. **53**, 04EL01 (7 pages) (2014)
18. Ishihara, H., Niitsu, K., Nakazato, K.: Analysis and experimental verification of DNA Single Base polymerization detection using CMOS FET-based redox potential sensor Array. Jpn. J. Appl. Phys. **54**(4S), 04DL05. (6 pages) (2015)
19. Niitsu, K., Yoshida, K., Nakazato, K.: Design and experimental demonstration of low-power CMOS magnetic cell manipulation platform using charge recycling technique. Jpn. J. Appl. Phys. **55**(3S2), 03DF13. (4 pages) (2016)
20. Tanaka, S., Niitsu, K., Nakazato, K.: A low-power inverter-based CMOS level-crossing a/D converter for low-frequency biosignal sensing. Jpn. J. Appl. Phys. **55**(3S2), 03DF10. (7 pages) (2016)
21. Yamaji, Y., Niitsu, K., Nakazato, K.: Design and experimental verification of low-voltage two-dimensional CMOS electrophoresis platform with 32×32 sample/hold cell Array. Jpn. J. Appl. Phys. **55**(3S2), 03DF07. (5 pages) (2016)
22. Niitsu, K., Kuno, T., Takihi, M., Nakazato, K.: Well-shaped microelectrode Array structure for high-density CMOS amperometric electrochemical sensor array. IEICE Trans. Electron. **E99-C**(6), 663–666 (2016)
23. K. Gamo, K. Niitsu, K. Nakazato: Noise-immune current-integration-based CMOS amperometric sensor platform with 1.2 μm x 2.05 μm electroless-plated microelectrode array for robust bacteria counting. In: Proc. IEEE Biomed. Circ. Syst. Conf. pp. 539–542 (2015)
24. K. Niitsu, A. Kobayashi, Y. Ogawa, M. Nishizawa, K. Nakazato. An energy-autonomous, disposable, big-data-based supply-sensing biosensor using Bio Fuel Cell and 0.23-V 0.25-μm Zero-Vth all-digital CMOS supply-controlled ring oscillator with inductive transmitter. In: Proc. IEEE Biomed. Circ. Syst. Conf. pp. 595–598 (2015)
25. S. Ota, K. Niitsu, H. Kondo, M. Hori, K. Nakazato: A CMOS sensor platform with 1.2 μm × 2.05 μm electroless-plated 1024 × 1024 microelectrode array for high-sensitivity rapid direct bacteria counting. In Proc. IEEE Biomedical Circuits and Systems Conf. pp. 460–463 (2014)
26. Niitsu, K., Sakurai, M., Harigai, N., Yamaguchi, T.J., Kobayashi, H.: CMOS circuits to measure timing jitter using a self-referenced clock and a cascaded time difference amplifier with duty-cycle compensation. IEEE J. Solid State Circuits. **47**(11), 2701–2710 (2012)
27. Niitsu, K., Harigai, N., Yamaguchi, T.J., Kobayashi, H.: A feed-forward time amplifier using phase detector and variable delay line. IEICE Trans. Electron. **E96-C**(6), 920–922 (2013)

28. Niitsu, K., Harigai, N., Kobayashi, H.: Design methodology for determining the number of stages in a cascaded time amplifier to minimize area consumption. IEICE Electron. Exp. **10**(11), 20130289 (2013)
29. Niitsu, K., Harigai, N., Yamaguchi, T.J., Kobayashi, H.: A low-offset cascaded time amplifier with reconfigurable inter-stage connection. IEICE Electron. Exp. **11**(10), 20140203 (2014)
30. Niitsu, K., Osawa, Y., Hirabayashi, D., Kobayashi, O., Yamaguchi, T.J., Kobayashi, H.: A CMOS PWM transceiver using self-referenced edge detection. IEEE Trans. Very Large Scale Integration (VLSI) Syst. **23**(6), 1145–1149 (2015)
31. Niitsu, K., Kang, S., Kulkarni, V.V., Ishikuro, H., Kuroda, T.: A 14 GHz AC-coupled clock distribution scheme with phase averaging technique using Sigle LC-VCO and distributed phase interpolators. IEEE Trans. Very Large Scale Integr (VLSI) Syst. (TVLSI). **19**(11), 2058–2066 (2011)
32. Niitsu, K., Sugimori, Y., Kohama, Y., Osada, K., Irie, N., Ishikuro, H., Kuroda, T.: Analysis and techniques for mitigating interference from power/signal lines and to SRAM circuits in CMOS inductive-coupling link for low-power 3D system integration. IEEE Trans. Very Large Scale Integr (VLSI) Syst. **19**(10), 1902–1907 (2011)
33. Niitsu, K., Kohama, Y., Sugimori, Y., Kasuga, K., Osada, K., Irie, N., Ishikuro, H., Kuroda, T.: Modeling and experimental verification of misalignment tolerance in inductive-coupling inter-Chip link for low-power 3D system integration. IEEE Trans. Very Large Scale Integr (VLSI) Syst. **18**(8), 1238–1243 (2010)
34. Saen, M., Osada, K., Okuma, Y., Niitsu, K., Shimazaki, Y., Sugimori, Y., Kohama, Y., Kasuga, K., Nonomura, I., Irie, N., Hattori, T., Hasegawa, A., Kuroda, T.: 3-D system integration of processor and multi-stacked SRAMs using inductive-coupling link. IEEE J. Solid-State Circ. **45**(4), 856–862 (2010)
35. Niitsu, K., Yuxiang, Y., Ishikuro, H., Kuroda, T.: A 33% improvement in efficiency of wireless inter-chip power delivery by thin film magnetic material for three-dimensional system integration. Jpn. J. Appl. Phys. **48**, 04C073. (5 pages) (2009)
36. Niitsu, K., Miura, N., Inoue, M., Nakagawa, Y.O., Tago, M., Mizuno, M., Sakurai, T., Kuroda, T.: Daisy chain transmitter for power reduction in inductive-coupling CMOS link. IEICE Trans. Electron. **E90-C**(4), 829–835 (2007)
37. Niitsu, K., Miura, N., Inoue, M., Nakagawa, Y., Tago, M., Mizuno, M., Ishikuro, H., Kuroda, T.: 60% power reduction in inductive-coupling inter-Chip link by current-sensing technique. Jpn. J. Appl. Phys. **46**(4B), 2215–2219 (2007)

http://www.springer.com/978-3-319-55344-3

Smart Sensors at the IoT Frontier
Yasuura, H.; Kyung, C.; Liu, Y.; Lin, Y.-L. (Eds.)
2017, VI, 378 p. 252 illus., 162 illus. in color., Hardcover
ISBN: 978-3-319-55344-3